Journal of Human Genetics (2017) 62, 473–480

www.nature.com/jhg

ORIGINAL ARTICLE

TBCD may be a causal gene in progressive neurodegenerative encephalopathy with atypical infantile spinal muscular atrophy

Toshio Ikeda[1], Akihiko Nakahara[2], Rie Nagano[3], Maiko Utoyama[1], Megumi Obara[1], Hiroshi Moritake[1], Tamayo Uechi[4], Jun Mitsui[5], Hiroyuki Ishiura[5], Jun Yoshimura[6], Koichiro Doi[6], Naoya Kenmochi[4], Shinichi Morishita[6], Ichizo Nishino[7], Shoji Tsuji[5] and Hiroyuki Nunoi[1]

Spinal muscular atrophy (SMA) is an autosomal recessive neurodegenerative disorder caused by survival motor neuron gene mutations. Variant forms of SMA accompanied by additional clinical presentations have been classified as atypical SMA and are thought to be caused by variants in as yet unidentified causative genes. Here, we presented the clinical findings of two siblings with an SMA variant followed by progressive cerebral atrophy, and the results of whole-exome sequencing analyses of the family quartet that was performed to identify potential causative variants. We identified two candidate homozygous missense variants, R942Q in the *tubulin-folding cofactor D* (*TBCD*) gene and H250Q in the *bromo-adjacent homology domain and coiled-coil containing 1* (*BAHCC1*) gene, located on chromosome 17q25.3 with an interval of 1.4 Mbp. The *in silico* analysis of both variants suggested that *TBCD* rather than *BAHCC1* was likely the pathogenic gene (*TBCD* sensitivity, 0.68; specificity, 0.97; *BAHCC1* sensitivity, 1.00; specificity, 0.00). Thus, our results show that *TBCD* is a likely novel candidate gene for atypical SMA with progressive cerebral atrophy. *TBCD* is predicted to have important functions on tubulin integrity in motor neurons as well as in the central nervous system.
Journal of Human Genetics (2017) **62,** 473–480; doi:10.1038/jhg.2016.149; published online 8 December 2016

INTRODUCTION

Infantile spinal muscular atrophy (SMA) is a frequent autosomal disease that specifically affects the motor neurons of the spinal anterior horn and lower cranial nerve nuclei.[1,2] Peripheral nerve involvement or other organ malformations are conventionally regarded as exclusion criteria for infantile SMA. However, recent reports indicate that although the neurological features are obvious early in childhood, the somatic features appear later in childhood, suggesting an apparent lack of boundaries between purely neurological and multiorgan syndromes over time.[1–3] SMA is caused by mutations in the *survival motor neuron 1* and *2* (*SMN1* and *SMN2*) genes on chromosome 5q13.[4] The homozygous absence of *SMN1* is responsible for SMA, whereas *SMN2* copy number is associated with the SMA phenotype.[4]

Atypical forms of the disease have been described. Patients with these forms have unusual additional neurological features (for example, diaphragmatic palsy) that are known as atypical SMA, SMA variant, non-5q-SMA entities or SMN1-negative proximal SMA.[5–8] Based on the mode of inheritance and involvement of other organs or peripheral nerves, atypical SMA types have been reported along with the causative genes, including pontocerebellar hypoplasia (PCH) with infantile SMA (PCH1A, *VRK1*; PCH1B, *EXSOC3*), SMA and progressive myoclonic epilepsy (PMESMA, *ASAH1*) and SMA with cranial nerve disorders.[5–13]

Progressive loss of neurological function along with the involvement of the central nervous system other than the motor neuron system is diagnosed as a neurodegenerative disease and is classified into five major categories: polioencephalopathies, leukoencephalopathies, corencephalopathies, spinocerebellopathies and diffuse encephalopathies.

Here, we presented cases of two siblings who showed symmetrical proximal neurogenic muscle atrophy complicated by cognitive dysfunction and progressive cerebral atrophy. We investigated the possibility that these siblings were affected by atypical SMA with autosomal recessive inheritance. To this end, we conducted whole-exome sequencing analyses on the two affected siblings and their parents, identifying variants in the *tubulin-folding cofactor D* (*TBCD*) gene and the *bromo-adjacent homology domain and coiled-coil containing 1* (*BAHCC1*) gene located on chromosome 17q25.3 with

[1]Division of Pediatrics, Department of Developmental and Urological-Reproductive Medicine Pediatrics, Faculty of Medicine, University of Miyazaki, Miyazaki, Japan; [2]Department of Pediatrics, National Hospital Organization Miyazaki Hospital, Miyazaki, Japan; [3]Department of Pediatrics, Aisenkai Nichinan Hospital, Miyazaki, Japan; [4]Frontier Science Research Center, University of Miyazaki, Miyazaki, Japan; [5]Department of Neurology, The University of Tokyo, Graduate School of Medicine, Tokyo, Japan; [6]Department of Computational Biology and Medical Sciences, Graduate School of Frontier Sciences, The University of Tokyo, Chiba, Japan and [7]Department of Neuromuscular Research, National Institute of Neuroscience, National Center of Neurology and Psychiatry, Tokyo, Japan
Correspondence: Dr T Ikeda, Division of Pediatrics, Department of Developmental and Urological-Reproductive Medicine Pediatrics, Faculty of Medicine, University of Miyazaki, Miyazaki 889-1692, Japan.
E-mail: toshio_ikeda@med.miyazaki-u.ac.jp
Received 15 July 2016; revised 5 November 2016; accepted 7 November 2016; published online 8 December 2016

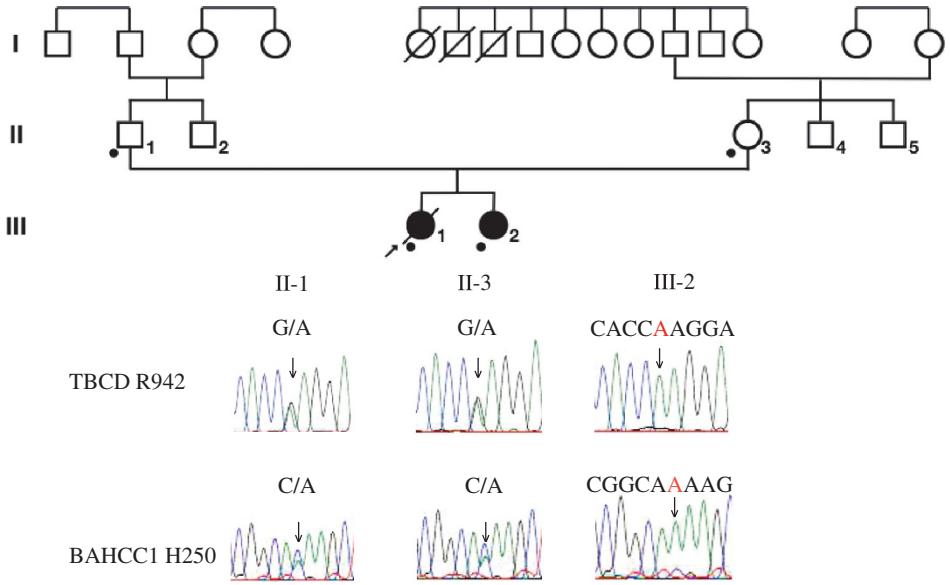

Figure 1 Family pedigree and chromatograms of two *de novo* variants identified in *tubulin-folding cofactor D* (*TBCD*) and *bromo-adjacent homology domain and coiled-coil containing 1* (*BAHCC1*). Participants with available whole-exome sequencing analysis are indicated by dots. Data were obtained by Sanger sequencing during the confirmation process. Direct nucleotide sequence analysis confirmed the *TBCD* variant (exon 31, c.2825G>A, R942Q) and the *BAHCC1* variant (exon 4, c.750C>A, H250Q).

an interval of 1.4 Mbp. Our results suggested that *TBCD* was the likely causative variant for these sibling cases.

MATERIALS AND METHODS

Ethics

All studies were performed with the informed consent of the patients' parents and the approval of the institutional review boards at the University of Miyazaki and the University of Tokyo.

Participants

Two Japanese familial patients with atypical SMA were enrolled in this study. Their pedigree chart is shown in Figure 1. The detailed clinical features of the sibling cases are provided in the Results section. Their parents were non-consanguineous.

Exome sequencing

Genomic DNA was extracted using standard protocols from peripheral blood leukocytes or the umbilical cord of the two patients and their parents. Whole-exome sequencing and bioinformatics analysis were performed on the two patients (cases 1 and 2) as previously described.[14,15] Briefly, exonic sequences were enriched using a SureSelect v4+UTRs kit (Agilent Technologies, Santa Clara, CA, USA) and subjected to massively parallel sequence analysis using an Illumina HiSeq 2500 sequencing system (Illumina, San Diego, CA, USA). The Burrows–Wheeler Aligner[16] and SAMtools[17] programs were used with the default parameter settings for alignment of raw reads and variation detection (human GRCh37/hg19). Single-nucleotide variants were filtered using 800 Japanese, in-house, healthy control exome data collected at the University of Tokyo.

SNP genotyping

Genotyping of single-nucleotide polymorphisms (SNPs) were performed using a Genome-Wide SNP Array 6.0 (Affymetrix). The availability of genomic DNA enabled genotyping of the genomic DNA of one patient (case 1) and the parents. SNP calling was performed using Genotyping Console software (Affymetrix, Santa Clara, CA, USA). PLINK software was used to obtain a pairwise identity-by-descent estimation.[18]

Sanger sequencing

Sanger sequencing was performed to validate each candidate variant detected by exome sequencing. The entire exon 31 from *TBCD* was amplified by PCR using an appropriate primer pair, TBCD-F 5′-GCATGTCCTCGTGGTGCTTG-3′ and TBCD-R 5′-GCCAATGATCTCGCCATGGC-3′, and AmpliTaq Gold (Life Technologies Japan, Tokyo, Japan). Similarly, the portion of exon 5 from *BAHCC1* harboring another candidate mutation was amplified by PCR using an appropriate primer pair, BAHCC1-F 5′-GAGTCAGTGCCAGCTGGTGTC-3′ and BAHCC1-R 5′-CTGCTGCCTCCTTGCACAG-3′ and AmpliTaq Gold.

Direct nucleotide sequence analysis was performed using the BigDye Terminator v3.1 kit and an ABI PRISM 3130 Genetic Analyzer instrument (Life Technologies, Carlsbad, CA, USA).

Database analyses

Sequences were compared with wild-type sequences using the online Basic Local Alignment Search Tool (BLAST; http://blast.ncbi.nlm.nih.gov/Blast.cgi) and the National Center for Biotechnology Information (NCBI) database (http://www.ncbi.nlm.nih.gov/homologene). Variants were tested for potential pathogenicity using the following bioinformatics software online tools: Polymorphism Phenotyping v2 (PolyPhen2; http://genetics.bwh.harvard.edu/pph2/index.shtml), Scale-Invariant Feature Transform (http://sift.jcvi.org/) and Align GVGD (http://agvgd.hci.utah.edu).[10,19,20] Protein structure predictions were performed using JPred 4 (http://www.compbio.dundee.ac.uk/jpred/) and I-TASSER (http://zhanglab.ccmb.med.umich.edu/).[21,22]

RESULTS

Case reports

Case 1. A 1-month-old girl was referred to our hospital with hypotonia and developmental problems. She was the first child of unrelated, healthy Japanese parents (Figure 1) and was born weighing 3080 g at 38 weeks of gestation via uterine inertia without fetal and neonatal hypoxemia.

Her vital signs and weight gain were normal, but she exhibited a frog-leg posture and head lag. She had no dysmorphic facial features or hepatosplenomegaly. Her mental status was alert and she was visually attentive. She cried weakly. Her eye positions were normal, there were no ocular deviations and her pupils were equal, round and reactive to light. Her face moved symmetrically. She was able to

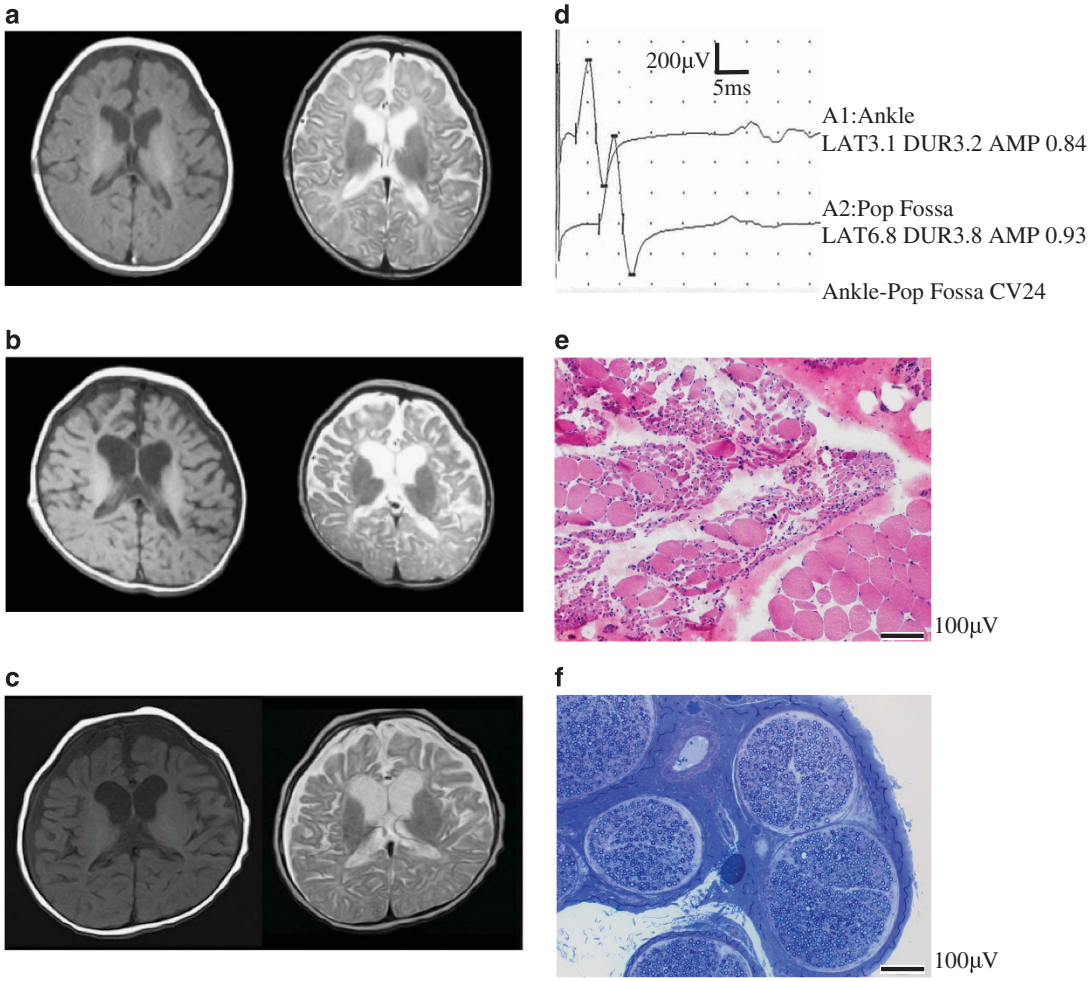

Figure 2 T1- and T2-weighted brain magnetic resonance imaging (MRI), nerve conduction study and muscle biopsy. (**a**) MRI of case 1 at 1 month of age showing normal findings. (**b**) At 7 months, T1- and T2- weighted brain MR images show progression of cerebral atrophy. Given the severe cerebral atrophy and less homogeneous hyperintensity of the white matter seen on T2-weighted imaging, the MRI findings indicate early-onset neurodegenerative disorder, in which impaired formation of myelin results from neuronal dysfunction.[49] (**c**) MRI results of case 2 at 6 months of age also reveal progressive cerebral atrophy with less hyperintensity of the white matter. However, this finding does not mean a primary hypomyelination.[49] (**d**) Nerve conduction study of case 1 at 9 months of age. The tibial nerve between the ankle and popliteal fossa shows reduced nerve conduction velocity of 24 m s^{-1} (normal 38.5 ± 5.5) and reduced compound muscle action potential of 0.93 mV (normal 14.1 ± 2.6). These findings can be accounted for by either axonal-dominant degeneration or motor unit reduction. Pop Fossa, popliteal fossa; LAT, latency (in ms); DUR, duration (in ms); AMP, amplitude (in mV); CV, conduction velocity (in m s^{-1}). (**e**) Biceps muscle biopsy from case 1 at 4 years of age showing large grouped atrophy with fiber hypertrophy, coincident with spinal muscular atrophy (SMA) findings (hematoxylin and eosin staining). (**f**) Sural nerve biopsy from case 1 at 4 years of age. This peripheral nerve biopsy specimen shows no axonal degeneration or swollen axons. Myelin sheaths are maintained (toluidine blue staining).

swallow during the initial visit. A high-arched palate was not noted. The tongue was midline and fasciculations were suspected. She had almost normal bulk with marked hypotonia. The Scarf sign was positive, with diffuse muscle weaknesses encompassing the trunk, limb symmetries and proximal muscle dominance. She was unable to lift her arms or legs against gravity, but had some movement of her hands and feet. Facial muscular weakness was noted. Pes equinus of both feet was noted. Involuntary movements were not observed. She exhibited some withdrawal and grimacing to pain. Although bilateral plantar flexor responses were absent, the Babinski reflex was positive, showing contraction of the extensor hallucis longus muscle. The Moro reflex was positive but weak. At her first visit, serum biochemical markers (creatine kinase, lactate, pyruvate, amino acid levels and other blood serology) were in the normal range. Brain magnetic resonance imaging (Figure 2a) results showed no obvious abnormal signal. No deletions or mutations in exons 7 and 8 of the *SMN* gene were identified from nucleotide sequence analyses of the PCR products, excluding typical infantile SMA.

At 3 months of age, tongue fasciculations were clearly apparent, and her voluntary smile and visual attention were lost. She was admitted again at 7 months because of a failure to thrive. Cerebral atrophy was confirmed by a computed tomography scan and also by brain magnetic resonance imaging (Figure 2b), with no findings of cerebellar atrophy or brainstem changes. Her head circumference was 0.23 s.d. at 1 month, but −2.1 s.d. at 8 months. Psychomotor retardation was clearly apparent and progressive. Symptomatic partial seizure was observed that was intractable to antiepileptic drugs. In addition to a weak cough and cry, respiratory distress and dysphagia with a bell-shaped chest and paradoxical respirations were confirmed at 9 months of age. She began to have difficulty swallowing. By 12 months, she was profoundly mentally and physically retarded, with a developmental quotient of <20. She was confined to bed, lost

spontaneous movements, communication or interaction with the environment, and she needed continuous tracheostomy positive pressure ventilation and tube nutrition. Although mild optic atrophy was observed, macular cherry-red spots and retinal pigmentary changes were not noted. Pupil responses, eye positions and ocular movements were normal, but reaction to light became incomplete. Optokinetic nystagmus, pursuit, saccade and eye contact were lost. These findings indicated progressively deteriorating visual functions, especially due to cortical visual impairment. Click-evoked auditory brainstem response thresholds at 9 months of age were 30 dB above normal adult hearing level (right) and 40 dB above normal adult hearing level (left). Latencies of waves I (right 1.68 ms, left 1.54 ms; normal 1.60 ± 0.46), III (right 3.70 ms, left 3.48 ms; normal 4.30 ± 0.50) and V (right 6.12 ms, left 5.28 ms; normal 6.63 ± 0.78) were obtained using 90 dB high-click stimuli at 9 months. These findings indicated normal auditory peripheral nerve and brainstem functions.

Reduced nerve conduction velocity ($27\ m\ s^{-1}$; normal 42.3 ± 6.4) and reduced compound muscle action potential (2.5 mV; normal 5.5 ± 2.0) were observed in the median nerve. Reduced nerve conduction velocity ($24\ m\ s^{-1}$; normal 38.5 ± 5.5) and reduced compound muscle action potential (0.93 mV; normal 14.1 ± 2.6) were also observed in the posterior tibial nerve (Figure 2d).

Lysosomal enzyme activities that are relevant to neurodegeneration involving the central nervous system and hypotonia (for example, glycosidases, lysosomal proteases and sulfatases) were in normal ranges. Normal serum levels of very long chain fatty acids excluded fatty acid β-oxidation cycle disorders, medium chain acyl-coenzyme A dehydrogenase deficiency, long chain 3-hydroxyacyl-coenzyme A dehydrogenase deficiency, very long chain acyl-coenzyme A dehydrogenase deficiency and glutaric acidemia type II. G-banded chromosomal analysis was normal. Cardiovascular, hepatic and renal functions were also normal. Echocardiography showed no signs of cardiomyopathy. At 3 years of age, a muscle biopsy specimen confirmed large grouped atrophy with fiber hypertrophy (Figure 2e). Sural nerve biopsy was normal upon optical microscopic examination (Figure 2f). She died of aspiration pneumonia at 6 years of age.

Case 2. The second patient was the younger sister of case 1 (Figure 1). She was born at 39 weeks of gestation via normal delivery without fetal and neonatal hypoxia, and weighed 3060 g. She was referred to our hospital at 6 months of age with hypotonia, developmental problems and pes equines. Her vital signs and weight gain were normal, but she exhibited a frog-leg posture and head lag. At the initial visit, her head circumference was within the normal range but became smaller than the reference range with increasing age. Her tongue was midline with fasciculations. Her respiratory condition, mental status, other symptoms and sensory and reflex responses were the same as those described for her sister. She also had severe psychomotor retardation. Intractable symptomatic partial seizure occurred at 8 months. Respiratory distress and dysphagia were progressive, and she needed a tracheostomy at 7 months. She has been mechanically ventilated to date, and is currently bedridden with profound mental retardation. She is still alive at the age of 7 with tracheostomy positive pressure ventilation, home-based respirator care.

Her serum biochemical markers were normal. Brain magnetic resonance imaging showed severe cerebral atrophy (Figure 2c), but no apparent cerebellar atrophy or brainstem changes. An interictal electroencephalogram showed occasional multi-foci paroxysmal sharp waves on a background activity of dysmorphic high-normal voltage delta and theta waves. This electroencephalogram did not indicate hypsarhythmia. Cardiovascular and hepatic functions were normal. A congenital solitary kidney was detected. At 7 years of age, eyelash and light reflexes were lost. Chromosomal G-band analysis and array comparative genomic hybridization (27K; Agilent Technologies, Santa Clara, CA, USA) found no chromosomal abnormality or copy number variations. She has lived a life similar to her elder sister.

Differential diagnoses were listed in the Supplementary Information.

Exome sequence analysis

A total of 142 rare protein-altering and splice-site variants, whose minor allele frequencies were $<0.5\%$ in 800 exomes from in-house, healthy controls, were identified in one or both cases. All variants in each participant were surveyed for compound heterozygous or homozygous variants that were consistent with an autosomal recessive trait in the family (Table 1).

Only two homozygous variants, c.750C>A (H250Q) in *BAHCC1* and c.2825G>A (R942Q) in *TBCD*, at 17q25.3 were shared between the siblings (Table 2). Their parents were heterozygous for the same variants of the alleles. R942Q in *TBCD* was present neither in the exomes from the 800 in-house, healthy controls nor in the Exome Aggregation Consortium data set, whereas H250Q in *BAHCC1* was observed in 2 of the 800 in-house, healthy controls (2 in 1600 alleles) (Figure 3).

In silico functional prediction of the variants

PolyPhen2 predicted the *BAHCC1* variant to be benign with a score of 0.000 (sensitivity, 1.00; specificity, 0.00) (Table 3). In contrast, the *TBCD* variant was predicted to be probably damaging, with a score of 0.995 (sensitivity, 0.68; specificity, 0.97). Moreover, Align GVGD predicted the *TBCD* variant as more likely than the *BAHCC1* variant to interfere with function. SIFT predicted both variants to affect protein functions, although with a postscript that the substitutions may have been predicted to affect functions because the sequences used were not sufficiently diverse. Protein structure predictions suggested that R942Q in TBCD may affect protein conformations and higher structures of an α-helix (Figure 4).

DISCUSSION

The siblings showed atypical SMA at a very early age during childhood, with hypotonia and muscle weakness indicating lower motor unit dysfunction, but, in addition, progressive complicated central nervous system dysfunctions. Severe infantile generalized weakness with tongue fasciculations and respiratory failure suggested an anterior horn disorder, such as SMA. A muscle biopsy specimen at 3 years of age confirmed grouped atrophy of muscles. The results of the nerve conduction study indicated that the tibial nerve showed

Table 1 Novel nonsynonymous variants detected in target regions of case 1 and case 2

	Reads	*Mapped reads*	*Mapped reads (unique)*	*Mapping rate (%)*	*Mapping rate (unique) (%)*	*Coverage*	*Coverage (unique)*
Case 1	79 409 125	111 355 984	109 060 264	99.2	97.2	156.3	153.1
Case 2	80 887 120	115 004 732	110 418 648	98.9	95.0	99.4	95.4

Table 2 Candidate homozygous variants detected in case 1 and case 2

Chromosome	*Position*	*Reference*	*Alternation*	*Zygosity*	*Mean allele frequency within in-house controls*	*Gene*	*Amino acid mutation*
Chr17	79 409 125	C	A	Homo	2/800 (0.25%)	*BAHCC1*	H250Q
Chr17	80 887 120	G	A	Homo	0/800	*TBCD*	R942Q

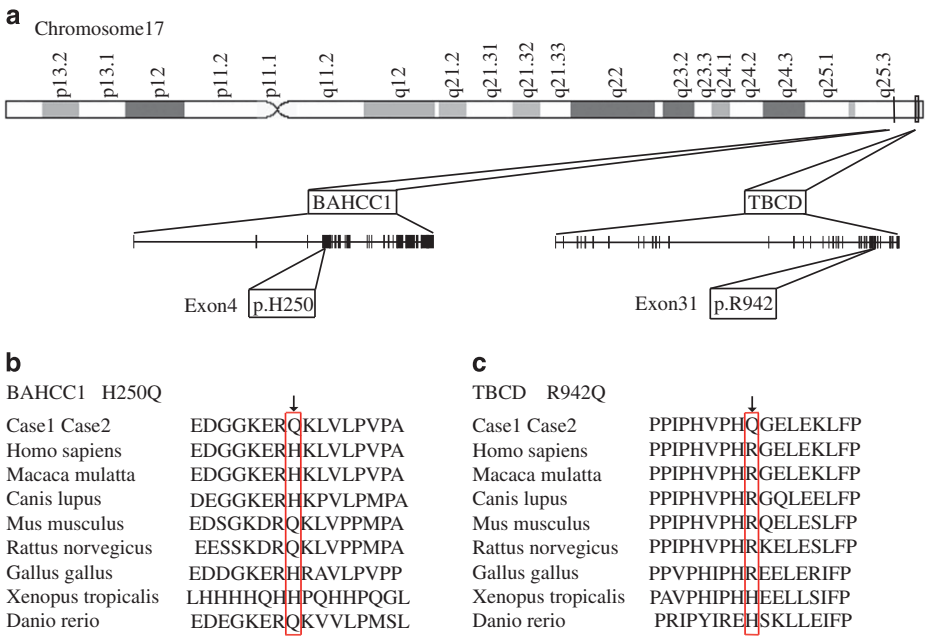

Figure 3 Identification of the putative causative variants in *tubulin-folding cofactor D* (*TBCD*) and *bromo-adjacent homology domain and coiled-coil containing 1* (*BAHCC1*). (**a**) Schematic of the *BAHCC1* gene, composed of 28 exons, and of the *TBCD* gene, composed of 1192 amino acids and 39 exons. (**b**, **c**) Partial amino acid sequence alignment reveals that (**b**) H250 and (**c**) R942 are evolutionally conserved among species.

Table 3 Predictions on the effect of missense substitutions in *BAHCC1* and *TBCD*

Gene	*Mutation*	*Polyphen2*	*SIFT*	*Align GVGD*
BAHCC1	H250Q	Benign	Affects protein function	Class C15[a]
TBCD	R942Q	Probably damaging	Affects protein function	Class C35[a]

[a]Classifiers are ordered along a spectrum (C0, C15, C25, C35, C45, C55 and C65) from most likely to interfere with function (C65) to least likely (C0).

axonal-dominant degeneration or motor unit reduction, whereas the results of the sural nerve biopsy suggested that the sural nerve was normal, indicating that the pathology was confined to motor neurons. Brain atrophy was progressive. The patient histories indicated severe developmental delay and regression, hypotonia, loss of visual attention, progressive feeding and respiratory problems and, ultimately, both patients became bedridden and lost any cognitive function at 3 years of age.

Progressive diffuse central nervous system disorders with cognitive (that is, developmental quotient <20) and motor dysfunctions are quite different from those observed in typical SMA and, furthermore, distinct from any other atypical forms of SMA, emphasizing the uniqueness of the clinical presentations of these sibling cases.

After differentiating motor neuron diseases from typical SMA and other disorders with similar clinical features, such as infantile hypotonia or psychomotor regression (see Supplement 1), we considered atypical SMA and amyotrophic lateral sclerosis.[23–26] Additional features, including arthrogryposis, myoclonic epilepsy, sensory neural deafness or pontocerebellar hypoplasia, were also investigated.[8–27] However, none of these features were observed, and amyotrophic lateral sclerosis was unlikely, because amyotrophic lateral sclerosis is usually regarded as an adult-onset neurodegenerative disorder.[27]

Many congenital neurodegenerative diseases or atypical SMA are known for distinct diagnoses of SMA1-like congenital illnesses; for example, SMA with respiratory distress (SMARD1), SMA with progressive myoclonic epilepsy (SMAPME) and pontocerebellar hypoplasia (PCH1A, PCH1B).[4–6] The siblings here exhibited some symptoms of SMARD1 (caused by *IGHMBP2* mutations), showing severe respiratory distress at the age of 1 to 6 months, but hemiparalysis of the diaphragm, a characteristic finding of SMARD1, was not observed.[11,28] Furthermore, SMARD1 does not complicate central nervous system disorders.[11,28]

Pontocerebellar hypoplasia exhibits the most similar clinical course to SMA, and refers to a group of severe neurodegenerative disorders that affect growth and function of the brainstem and cerebellum, eventually resulting in little or no development.[8,29,30] Different types of pontocerebellar hypoplasia are classified based on clinical findings and the spectra of pathological changes.[8,29,30] Type 1 PCH is characterized by central and peripheral motor dysfunction associated with anterior horn cell degeneration, and resembles infantile SMA, usually leading to early death.[29,30] With type 2 PCH, there is progressive microcephaly from birth combined with extrapyramidal dyskinesias.[29,30] Marked PCH and progressive cerebral atrophy are revealed by brain computed tomography. Here, the siblings showed microcephaly, progressive cerebral atrophy (but not spastic palsy), severe extrapyramidal dyskinesia and failure to acquire any voluntary skills. There are many other types of PCH (2 – 7), but hyperreflexia, optic atrophy (PCH3),

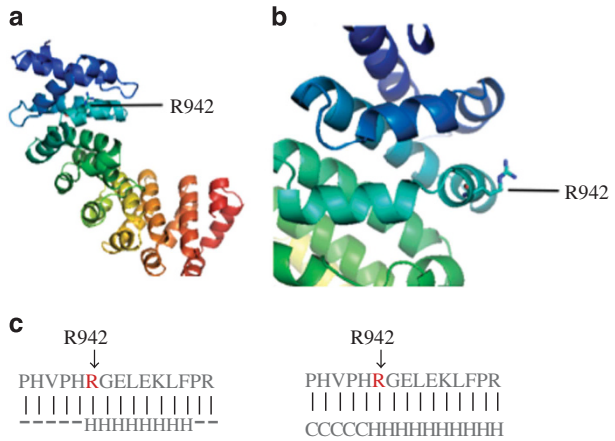

Figure 4 Structure models of tubulin-folding cofactor D (TBCD) showing the R942Q variant. (**a**, **b**) TBCD protein structure from amino acids 865 to 1170; (**a**) and (**b**) show the same structures observed at different angles. PBD ID was downloaded using the Mod database.[50] R942Q is located on the protein surface and is part of a helical structure, suggesting it may be involved in protein–protein or intermolecular interactions by causing loss of a positively charged amino acid.[19,49] R942Q is represented using a stick, whereas the other structures are shown as cartoons. (**c**) Protein structure predictions using JPred (left) and I-TASSER (right).[22,27] R942Q likely influences an α-helix. H, α-helix; C, coil.

joint contracture, olivopontocerebellar hypoplasia (PCH4), cerebellar hypoplasia apparent in the second trimester, seizures (PCH5) and mitochondrial respiratory chain defects (PCH6) were not confirmed in the present cases.[29,30] Genital abnormalities associated with PCH (PCH7) are only observed in patients with the XY karyotype.[30]

To the best of our knowledge, the same clinical presentation observed here has not been previously reported; hence, we conducted exome sequencing of the family quartet: the patients (cases 1 and 2) and their parents. Assuming autosomal recessive inheritance, we searched for genes with compound heterozygous or homozygous protein-altering or splice-site variants with minor allele frequencies of $<0.5\%$ in the exomes from the 800 in-house, healthy controls, and found that the siblings carried two homozygous missense variants, R942Q in *TBCD* and H250Q in *BAHCC1*. Their parents had the same variants of these genes in heterozygous states. R942Q in *TBCD* is a novel variant, whereas H250Q in *BAHCC1* was observed in 2 of the 800 in-house healthy controls, suggesting that R942Q in *TBCD* is more likely than H250Q in *BAHCC1* to be the causative variant. This notion was further supported by the following findings. (1) A variant of *Drosophila TBCD* in projection neurons leads to microtubule destruction and axonal degeneration.[31] (2) Murine *Tbce* gene mutants, homologs of human *tubulin-folding cofactor E* (*TBCE*), show phenotypic characteristics of SMA-like motor neuropathy.[32–34] (3) In *Smn*-knockdown cells and SMA-like mice, microtubule density and β-tubulin levels are reduced.[35] The α/β-tubulin heterodimer formation requires participation of a series of chaperone proteins (tubulin-folding cofactors A–E) that function downstream of cytosolic chaperonin as a heterodimer assembly machine, and of which, TBCD forms one of the assemblies.[36] The efficiency with which TBCD affects tubulin disruption *in vivo* depends on its origin: overexpression of bovine TBCD efficiently destroys tubulin and microtubules in cultured cells.[36] Interestingly, TUBA4A has recently been reported to be associated with familial amyotrophic lateral sclerosis, supporting that tubulin integrity is essential in motor neurons.[37] (4) In addition, in many syndromes of conventionally grouped purely neurological disorders, extraneurological or other neurological complications will appear later in childhood.[2,3] Giant axonal neuropathy (GAN), related to GAN (gigaxonin) mutations, is known as one of the most recognizable neurodegenerative disorders.[3] GAN controls vimentin organization through a tubulin chaperone (TBCB, TBCE)-independent pathway.[38] Although our cases differed from GAN because of our peripheral nerve biopsy findings, these reports may indicate a relationship between tubulin chaperones and neurodegenerative disorders.

According to the protein structure models of Pymol (http://www.pymol.org/) and predicted protein structures, R942 is involved in protein–protein interactions in structured helices,[39,40] and evolutionally conserved among species (Figure 3). The R942Q variant is suspected to influence protein conformation and function by changing a positive to a neutral amino acid on the protein surface (Figure 4).

Although R942Q has not been reported in public databases, two missense changes involving adjacent residues have been annotated (rs753751532, H941Y; rs8072406, G943V).[40] The reasons why H941Y and G943V have been reported as not affecting pathogenesis may be that H941Y does not form a helical structure (Figure 4) and possibly does not highly affect protein structure,[41] and G943V does not alter charged amino acids. Both glycine and valine are nonpolar hydrophobic amino acids.[41] Therefore, we predict that R942Q causes the loss of the electrostatic stability of the TBCD protein because of the alteration from a positive to a neutral charge in an amino acid.[42]

The *BAHCC1* gene may also be causative in our cases because mice with a knockout of the human *BAHCC1* ortholog (KIAA 1447) have overt motor deficits.[43] However, *in silico* amino acid prediction analyses of both homologous missense mutations using PolyPhen2 and Align GVGD showed that R942Q in *TBCD* was more likely (sensitivity, 0.68; specificity, 0.97) than H250Q in *BAHCC1* (sensitivity, 1.00; specificity, 0.00) to be causative.[18,19] Guidelines for using prediction methods recommend the application of several tools, if possible. Herein, we analyzed the results using three different prediction tools.[44]

TBCD and *BAHCC1* are both located on chromosome 17q25.3 at an interval of 1.4 Mbp. Moreover, there is a run of homozygosity in the 1.8 Mbp region (chr17 79 429 228-qter) that includes *TBCD* and *BAHCC1* as observed by exome and high-density SNP results (data not shown), raising the possibility that both parents inherited the variants in *TBCD* and *BAHCC1* from a common ancestral individual. Identity-by-descent estimation of the parents from the SNP data, however, did not suggest that the parents were closely related, because the pi-hat value, which estimates the proportion of identity by descent between them, was 0.0075. Although R942Q in *TBCD* is most likely the causative variant, as discussed above, we cannot rule out the possibility of more complex models (that is, *TBCD* and *BAHCC1* coexpression, or autosomal dominant transmission because of parental germinal mosaicism). Further functional analyses using *in vivo* and *in vitro* models will be necessary to investigate how these mutations are involved in the clinical presentation.

Recently, three papers describing the similar cases with *TBCD* variation were published.[45–47] The patients of these papers were described as early-onset cortical atrophy, postnatal microcephaly and developmental delay/regression.[45–47] Several cases appeared as postnatal growth retardation, muscle weakness/atrophy, respiratory failure, seizures, optic nerve atrophy, progressive spasticity or severe dystonia.[45–47] However, our cases would be most severe neurodegenerative conditions as in our paper.

These papers include some functional aspects of the linkage between the disease phenotype and *TBCD* variation, and they determined *TBCD* as a causal gene of their patients' disease because the phenotypes were quite similar to that of previous report.[45–47]

In conclusion, a homozygous mutation in *TBCD*, which encodes tubulin cofactor, is likely responsible for a novel and severe neurodegenerative disorder.

Accession numbers and reference sequences

Nucleotide sequence data reported are available in the DNA Data Bank of Japan database under the accession numbers LC071985 and LC072713.

Reference sequences are available from NCBI for the *Homo sapiens TBCD* mutation (NC_000017.10 chromosome 17 reference GRCh primary Assembly; NC_000017.11 chromosome 17 reference GRCh primary Assembly; and NCBI Reference Sequence: NG_011721.1) and the *BAHCC1* mutation (NC_000017.10 chromosome 17 reference GRCh primary Assembly; and NC_000017.11 chromosome 17 reference GRCh primary Assembly).[48]

CONFLICT OF INTEREST

The authors declare no conflict of interest.

ACKNOWLEDGEMENTS

We thank the individuals with atypical SMA and their family for their participation in this study. We also thank Drs K Kanako and S Yuko (Department of Neuromuscular Research, National Institute of Neuroscience, National Center of Neurology and Psychiatry) for their helpful comments on the sural nerve biopsy, and Dr K Shiomi (Division of Neurology, Respirology, Endocrinology and Metabolism, Department of Internal Medicine, University of Miyazaki) for help with the nerve conduction study. This work was supported in part by Grants-in-Aid for Scientific Research (KAKENHI) for Scientific Research on Innovative Areas (Exploring Molecular Basis for Brain Diseases Based on Personal Genomics), Priority Areas (Applied Genomics), Integrated Database Project and Scientific Research (A) from the Ministry of Education, Culture, Sports, Science and Technology of Japan, and by a Clinical Research Grant from Miyazaki University Hospital.

Author contributions: TI confirmed the diagnosis in each participating patient, conceived the study, participated in the sequence alignment, designed and performed the experiments, analyzed the data, contributed reagents/materials/analysis tools and drafted the manuscript. AN confirmed the diagnosis for the participating patient designated as case 2, conceived the study, participated in the sequence alignment, designed and performed the experiments, analyzed the data and helped to draft the manuscript. RN confirmed the diagnosis for the participating patient designated as case 1. MU performed the experiments. MO designed and performed the experiments and analyzed the data. HM conceived the study and helped to draft the manuscript. TU conceived and designed the experiments. JM, HI, JY, KD and SM performed the experiments and contributed reagents/materials/analysis tools. NK and NI conceived and designed the experiments. ST conceived and designed the experiments and contributed reagents/materials/analysis tools and drafted manuscript. HN conceived the study, and participated in its design and coordination and helped to draft the manuscript. All authors read and approved the final manuscript.

1 Rudnik-Schöneborn, S., Goebel, H. H., Schlote, W., Molaian, S., Omran, H., Ketelsen, U. *et al.* Classical infantile spinal muscular atrophy with SMN deficiency causes sensory neuronopathy. *Neurology* **60**, 983–987 (2003).
2 Pierre, L. & Jonathan, B. Early onset (childhood) monogenic neuropathies. *Handb. Clin. Neurol.* **115**, 863–891 (2013).
3 Pierre, L., Jonathan, B. & Peter, D. Hereditary motor-sensory, motor, and sensory neuropathies in childhood. *Handb. Clin. Neurol.* **113**, 1413–1432 (2013).
4 Wirth, B. An update of the mutation spectrum of the survival motor neuron gene (SMN1) in autosomal recessive spinal muscular atrophy (SMA). *Hum. Mutat.* **15**, 228–237 (2000).
5 Ursula, F. M., Katja, G., Anja, H., Christine, S., Klaus, Z., Christoph, B. *et al.* Severe spinal muscular atrophy variant associated with congenital bone fractures. *J. Child. Neurol.* **17**, 718–721 (2002).
6 Klaus, Z. & Sabine, R. S. 93rd ENMC international workshop: non-5q-spinal muscular atrophies (SMA) – clinical picture (6–8 April 2001, Naarden, The Netherlands). *Neuromuscul. Disord.* **13**, 179–183 (2003).
7 Nathalie, G., Jean-Marie, C., Jean-Christophe, C., Jean-Francois, H., Sylvie, J. & Louis, V. *Brain. Dev.* **30**, 169–178 (2008).
8 Kristien, P., Teodora, C. & Albena, J. Clinical and genetic diversity of SMN1-negative proximal spinal muscular atrophies. *Brain* **137**, 2879–2896 (2014).
9 Rudnik-Schöneborn, S., Forkert, R., Hahnen, E., Wirth, B. & Zerres, K. Clinical spectrum and diagnostic criteria of infantile spinal muscular atrophy: further delineation on the basis of SMN gene deletion findings. *Neuropediatrics* **27**, 8–15 (1996).
10 Kumar, P., Henikoff, S. & Ng, P. C. Predicting the effects of coding non-synonymous variants on protein function using the SIFT algorithm. *Nat. Protoc.* **4**, 1073–1081 (2009).
11 Kaindl, A. M., Guenther, U. P., Rudnik-Schöneborn, S., Varon, R., Zerres, K., Schuelke, M. *et al.* Spinal muscular atrophy with respiratory distress type 1 (SMARD1). *J. Child. Neurol.* **23**, 199–204 (2008).
12 Grohmann, K., Markus, S., Alexander, D., Katrin, H., Barbara, L., Coleen, A. *et al.* Mutations in the gene encoding immunoglobulin μ-binding protein 2 cause spinal muscular atrophy with respiratory distress type 1. *Nat. Genet.* **29**, 75–77 (2001).
13 Guenther, U. P., Handoko, L., Laggerbauer, B., Jablonka, S., Chari, A., Alzheimer, M. *et al.* IGHMBP2 is a ribosome-associated helicase inactive in the neuromuscular disorder distal SMA type 1 (DSMA1). *Hum. Mol. Genet.* **18**, 1288–1300 (2009).
14 Ishiura, H., Fukuda, Y., Mitsui, J., Nakahara, Y., Ahsan, B., Takahashi, Y. *et al.* Posterior column ataxia with retinitis pigmentosa in a Japanese family with a novel mutation in FLVCR1. *Neurogenetics* **12**, 117–121 (2011).
15 Ishii, A., Saito, Y., Mitsui, J., Ishiura, H., Yoshimura, J., Arai, H. *et al.* Identification of ATP1A3 mutations by exome sequencing as the cause of alternating hemiplegia of childhood in Japanese patients. *PLoS ONE* **8**, e56120 (2014).
16 Heng, L. & Richard, D. Fast and accurate short read alignment with Burrows–Wheeler transform. *Bioinformatics* **25**, 1754–1760 (2009).
17 Heng, L., Bab, H., Alec, W., Tim, F., Jue, R., Nils, H. *et al.* The Sequence Alignment/Map format and SAMtools. *Bioinformatics* **25**, 2078–2079 (2009).
18 Shaun, P., Benjamin, N., Kathe, T. B., Lori, T., Manuel, A. R. F., David, B. *et al.* PLINK: a tool set for whole-genome association and population-based linkage analyses. *Am. J. Hum. Genet.* **78**, 615–628 (2007).
19 Adzhubei, I. A., Schmidt, S., Peshkin, L., Ramensky, V. E., Gerasimova, A., Bork, P. *et al.* A method and server for predicting damaging missense mutations. *Nat. Methods* **7**, 248–249 (2010).
20 George, D. C., Chakraborty, C., Haneef, S. A., Nagasundaram, N., Chen, L., Zhu, H. *et al.* Evolution- and structure-based computational strategy reveals the impact of deleterious missense mutations on MODY 2 (maturity-onset diabetes of the young, type 2). *Theranostics* **4**, 366–385 (2014).
21 Drozdetskiy, A., Cole, C., Procter, J. & Barton, G. J. JPred4: a protein secondary structure prediction server. *Nucleic. Acids. Res.* **43**, 389–394 (2015).
22 Yang, J. & Zhang, Y. I-TASSER server: new development for protein structure and function predictions. *Nucleic. Acids. Res.* **43**, 174–181 (2015).
23 Michel, V. J. in *Nelson Textbook of Pediatrics* 17th edn (eds Richard E. B., Robert M. K. & Hal B. J.) 2029–2035 (Elsevier, Saunders, Philadelphia, PA, USA, 2001).
24 Gerald, M. F. in *Clinical Pediatric Neurology: A Signs and Symptoms Approach* 4th edn (Elsevier, Saunders, Philadelphia, PA, USA, 2001).
25 JEric, P. G. in *Fenichel's Clinical Pediatric Neurology: A Signs and Symptoms Approach* 7th edn (Elsevier, Saunders, Philadelphia, PA, USA, 2013).
26 Sasaki, M., Sugai, K. & Inagaki, M. in *National Center of Neurology and Psychiatry, Department of Child Neurology, A Manual of Diagnosis And Treatment* 3rd edn (Shindantochiryousha, Tokyo, Japan, 2015).
27 Drik, B., Kevin, T. & Martin, R. T. Advances in motor neurone disease. *J. R. Soc. Med.* **107**, 14–21 (2014).
28 Matthew, P., Henry, H., Jean, J., Quen, M., Brian, H., Mary, R. *et al.* Severe infantile neuropathy with diaphragmatic weakness and its relationship to SMARD1. *Brain* **126**, 2682–2692 (2003).
29 Stephen, M. M., Kaashif, A. A., Yalda, M., Erin, L. M., Millan, S. P., David, C. *et al.* Pontocerebellar hypoplasia: review of classification and genetics, and exclusion of several genes known to be important for cerebellar development. *J. Child. Neurol.* **26**, 288–294 (2011).
30 Yasmin, N., Peter, Bwee, G. B., Tien, P. T. & Frank, B. Classification, diagnosis and potential mechanisms in pontocerebellar hypoplasia. *Orphanet. J. Rare. Dis.* **6**, 50 (2011).
31 Okumura, M., Sakuma, C., Miura, M. & Chihara, T. Linking cell surface receptors to microtubules: tubulin folding cofactor D mediates Dscam functions during neuronal morphogenesis. *J. Neurosci.* **35**, 1979–1990 (2015).
32 Martin, N., Jaubert, J., Gounon, P., Salido, E., Haase, G., Szatanik, M. *et al.* A missense mutation in TBCE causes progressive motor neuronopathy in mice. *Nat. Genet.* **32**, 443–447 (2002).
33 Winnie, C., Wim, W., Martin, P., Karoly, S., Jan, W., Edwin, R. *et al.* Hypoparathyroidism-retardation-dysmorphism syndrome in a girl: a new variant not

caused by a TBCE mutation—clinical report and review. *Am. J. Med. Genet.* **140A**, 611–617 (2006).
34 Don, W. C., Koji, Y. & Pascale, B. Gigaxonin controls vimentin organization through a tubulin chaperone-independent pathway. *Hum. Mol. Genet.* **18**, 1384–1394 (2009).
35 Hsin-Lan, W., Yuan-Ta, L., Chen-Hung, T., Sue, L. C., Hung, L., Hsiu, M. H. *et al.* Stathmin, a microtubule-destabilizing protein, is dysregulated in spinal muscular atrophy. *Hum. Mol. Genet.* **19**, 1766–1778 (2010).
36 Guoling, T., Simi, T. & Nicholas, J. C. Effect of TBCD and its regulatory interactor Arl2 on tubulin and microtubule integrity. *Cytoskeleton* **67**, 706–714 (2010).
37 Smith, B. N., Ticozzi, N., Fallini, C., Gkazi, A. S., Topp, S., Kenna, K. P. *et al.* Exome-wide rare variant analysis identifies TUBA4A mutations associated with familial ALS. *Neuron* **84**, 324–331 (2014).
38 Cleveland, D. W., Yamanaka, K. & Bomont, P. Gigaxonin controls vimentin organization through a tubulin chaperone-independent pathway. *Hum. Mol. Genet.* **18**, 1384–1394 (2009).
39 Grynberg, M., Jaroszewski, L. & Godzik, A. Domain analysis of the tubulin cofactor system: a model for tubulin folding and dimerization. *BMC Bioinformatics* **4**, 46 (2003).
40 Groves, M. R. & Barford, D. Topological characteristics of helical repeat proteins. *Curr. Opin. Struct. Biol.* **9**, 383–389 (1999).
41 National Center for Biotechnology Information. Single Nucleotide Polymorphism Database (dbSNP) (1998). http://www.ncbi.nlm.nih.gov/SNP/. Accessed 22 May 2016.
42 Anders, L., Lars, L., Jure, P., Goran, L., Poul, N. & Morten, K. *Textbook of Structural Biology* (World Scientific, Toh Tuck Link, Singapore, 2009).
43 Nakayama, M., Iida, M., Koseki, H. & Ohara, O. A gene-targeting approach for functional characterization of KIAA genes encoding extremely large proteins. *FASEB J* **20**, 1718–1720 (2006).
44 Vihinen, M. Guidelines for reporting and using prediction tools for genetic variation analysis. *Hum. Mutat.* **7**, 248–249 (2010).
45 Noriko, M., Ryoko, F., Chihiro, O., Takahiro, C., Masayuki, M., Hiroshi, S. *et al.* Biallelic *TBCD* mutations cause early-onset neurodegenerative encephalopathy. *Am. J. Hum. Genet.* **99**, 950–961 (2016).
46 Elisabetta, F., Marcello, N., Serena, C., Isabelle, T., Margaret, G. A., Alessandro, C. *et al.* Biallelic mutations in *TBCD,* encoding the tubulin folding cofactor D, perturb microtubule dynamics and cause early-onset encephalopathy. *Am. J. Hum. Genet.* **99**, 962–973 (2016).
47 Edvardson, S., Tian, G., Cullen, H., Vanyai, H., Ngo, L., Bhat, S. *et al.* Infantile neurodegenerative disorder associated with mutations in TBCD, an essential gene in the tubulin heterodimer assembly pathway. *Hum. Mol. Genet.* (e-pub ahead of print 29 August 2016; doi:10.1093/hmg/ddw292) (in press).
48 National Center for Biotechnology Information. Gene (2003). http://www.ncbi.nlm.nih.gov/gene/. Accessed 12 February 2015.
49 Wolf, N. I. & van der Knaap, M. S. AGC1 deficiency and cerebral hypomyelination. *N. Engl. J. Med.* **361**, 1997–1998 (2009).
50 University of California San Francisco Database of Comparative Protein Structure Models (ModBase) (2009) http://modbase.compbio.ucsf.edu/modbase-cgi/index.cgi. Accessed 15 February 2015.

Supplementary Information accompanies the paper on Journal of Human Genetics website (http://www.nature.com/jhg)